

Quantitative Analysis of In-Field Defects in Image Sensor Arrays

Jenny Leung, Jozsef Dudas, Glenn H. Chapman
School of Engineering Science,
Simon Fraser University,
Burnaby, B.C., Canada, V5A 1S6
jla98@sfu.ca, jdudas@sfu.ca,
glennc@ensc.sfu.ca

Israel Koren, Zahava Koren
Dept. of Electrical and Computer
Engineering,
University of Massachusetts,
Amherst, MA, 01003
koren{zkoren}@ecs.umass.edu

Abstract

Growth of pixel density and sensor array size increases the likelihood of developing in-field pixel defects. An ongoing study on defect development in imagers has now provided us sufficient data to be able to quantify characteristics of defect growth. Preliminary investigations have shown that defects are distributed randomly and the closest distance between two defective pixels is approximately 79-340 pixels apart. Furthermore, from an observation of 98 cluster-free defects, the diameter of the defect is estimated to be less than 2.3% of a pixel size at 99% confidence level. The fact that no defect clusters were found in the study of various digital cameras allows us to conclude that defects are not likely to be related to material degradation or imperfect fabrication but are due to environmental stress such as radiation. Furthermore, as verified by a statistical study, the absence of defect clustering provides information on the size of defects and insight into the nature of the defect development.

1. Introduction

With the advancement in digital imager technology, imagers have been employed in numerous fields for their ability to capture vibrant and fine detail images. Like all microelectronic devices, defects develop during the lifetime of imagers and result in defective sensors. The large area and analog nature of imagers means that although defect development in digital circuits is quite rare on a per pixel bases, defect occurrences in a given imager are quite common. Indeed, our measurements show that the majority of cameras develop defects over time. An extensive study by a major manufacturer of Charge Coupled Device (CCD) image sensors has conclusively confirmed the growth of in-field defects in terrestrial environments at both high altitude and sea level [1]. Here, we expand on that work by including data from other imaging technologies and cameras subjected to more varied environmental conditions. We also look in depth at the imaging and growth characteristics of individual defects to suggest potential defect causing mechanisms.

In our previous work, samples of digital photo cameras were subjected to laboratory calibration techniques in order to characterize the behavior of in-field defects [2]. The same study also successfully pinpointed the time, within some error, at which each defect was observed to develop. From that preliminary data, several key observations were made about one specific class of in-field defects, namely, hot pixels. First, hot pixels appear to develop suddenly and do not heal or disappear over time. Thus, defects continue to accumulate throughout the entire lifetime of the sensor and will eventually limit the imaging performance of the system. Furthermore, preliminary investigation of the spatial distribution of hot-pixels suggests they follow a uniform random distribution without evidence of clustering or multiple-pixel defects.

Detailed analysis of each of these characteristics can be used to further understand the defect growth rate, defect distribution, and approximate size of the defective area. In this paper we build on this previous work by adding additional analytical techniques while extending significantly the number of cameras we have studied to increase the statistical relevance of the data, thus enabling us to assign quantitative values to the behavior of in-field defects.

2. Defect description and detection

Calibrated uniform illuminations are used to search for the existence of particular defect types, to estimate the relative prevalence of each defect type, and to offer more detailed insight into the behavior of such defects. In particular, fully-stuck, partially-stuck, abnormal-sensitivity and hot pixel are the types of defects we examine.

Equations (1)-(4) describe the expected output of each defect type considered, where I_{photo} is the generated photocurrent, $T_{Integration}$ is the exposure duration and $f(I_{photo}, T_{integration})$ denotes the normalized pixel output. Fully-stuck defects are pixels each of which maintains some constant value c under any illumination as described by (1).

$$f_{Fully-stuck}(I_{photo}, T_{Integration}) = c, \quad 0 < c < 1 \quad (1)$$

For example, all stuck dark pixels have $c=0$ while all stuck bright (high) pixels have $c=1$.

Partially-stuck defects are described by (2), where the output is a function of the illumination $I_{photo} \cdot T_{Integration}$, and an illumination-independent offset b specific to that pixel.

$$f_{Partially-Stuck}(I_{photo}, T_{Integration}) = I_{photo} T_{Integration} + b \quad (2)$$

Abnormal-sensitivity defects can be described by Equation (3), where we model the defect as a linear function of the illumination $I_{photo} \cdot T_{Integration}$, the sensitivity m , and the offset b .

$$f_{Abnormal-Sensitivity}(I_{photo}, T_{Integration}) = m \cdot I_{photo} T_{Integration} + b \quad (3)$$

A series of uniform bright-field illuminations are used to identify the above defect types. For example, stuck and partially-stuck pixels will always give the same output under all illuminations. Abnormal-sensitivity defects are identified by comparing the illumination response of neighboring pixels. Since close proximity pixels should exhibit closely matched sensitivity, variations in sensitivity indicate the presence of a defect.

Uniquely important to imagers is an additional defect type, the hot pixel. This defect has a significant illumination-independent component and can be described by Equation (4), where I_{Dark} is the dark current presented at the pixel and the product $m \cdot I_{Dark} \cdot T_{Integration}$ represents the effect of dark current integrated at the output of that particular pixel. Hot pixels can be identified by observing the response of a pixel under no illumination with increasing exposure time (i.e., multiple images at varied exposure durations).

$$f_{Hot-Pixel}(I_{photo}, I_{Dark}, T_{Integration}) = m \cdot (I_{photo} T_{Integration} + I_{Dark} T_{Integration}) + b \quad (4)$$

3. Experimentally measured defect characteristics

Continuing from a previous study [2], an extended number of semi-professional cameras were analyzed for the defect types described in the previous section. The summary of the set of tested cameras used for the analysis appears in Table 1. These devices are representative of high performance large area devices and include sensors from both major imaging technologies: Charge Coupled Device (CCD) and Active Pixel Sensor (APS). The frequency of occurrence of every defect type in each of the 10 tested cameras is summarized in Table 2.

Our tests identified no fully-stuck defects or abnormal-sensitivity defects, suggesting that in-field defect mechanisms in this class of cameras are unlikely to lead to these defects (at least in the time frame we considered). However, significant quantities of in-field hot pixels were identified in 9 out of the 10 devices. The next 3 sections provide a quantitative analysis of the different aspects of the observed defects.

Table 1. Summary of tested cameras.

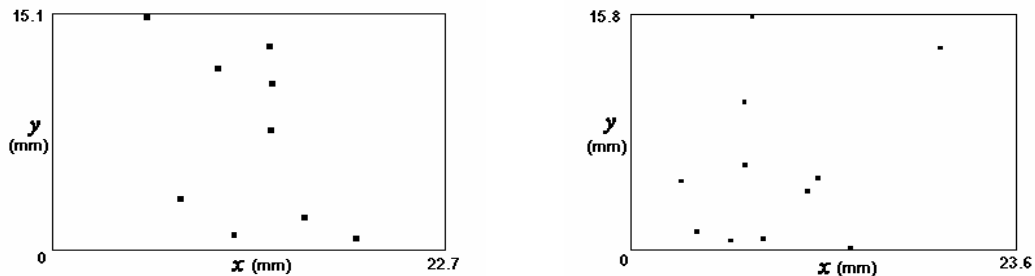
Camera	Sensor Type	# of Pixels	Sensor Size (mm × mm)	Age (years)
A	CMOS APS	6.3 M	22.7 × 15.1	3.0
B	CCD	6.0 M	23.7 × 15.5	2.5
C	CCD	10.0 M	23.6 × 15.8	0.5
D	CMOS APS	12.2 M	23.7 × 15.7	2.0
E	CCD	5.3 M	23.7 × 15.5	5.0
F	CMOS APS	6.0 M	22.7 × 15.1	1.5
G	CMOS APS	8.0 M	22.2 × 14.8	0.5
H	CCD	6.0 M	23.7 × 15.5	2.0
I	CCD	10.0 M	23.6 × 15.8	0.7
J	CCD	10.0 M	23.6 × 15.8	0.7

Table 2. Summary of defects found in tested cameras.

Camera	Number of defects found								
	Stuck				Abnormal sensitivity	Hot			Total
	Low	High	Partial	Total		No offset	W/ offset	Total	
A	0	0	7	7	0	2	7	9	9
B	0	0	0	0	0	17	0	17	17
C	0	0	5	5	0	6	5	11	11
D	0	0	0	0	0	0	0	0	0
E	0	0	0	0	0	26	0	26	26
F	0	0	2	2	0	0	2	2	2
G	0	0	0	0	0	3	0	3	3
H	0	0	0	0	0	7	0	7	7
I	0	0	10	10	0	2	10	12	12
J	0	0	9	9	0	2	9	11	11
<i>Cumulative total</i>									98

4. Spatial distribution of defects

The coordinates of defective pixels were recorded and used to create defect maps, which were then analyzed to determine the spatial distribution of defects in each sensor. Sample defect maps from two tested cameras are shown in Figure 1.



(a) Camera A (APS)

(b) Camera C (CCD)

Figure 1. Map of hot-pixel defects from (a) camera A and (b) Camera C

Simple visual inspection of these maps suggests that defects develop individually, rather than in clusters, and are distributed uniformly across the sensor area. These aspects of the defect distributions are further investigated next.

When a defect is related to material degradation, the neighbors of a defective pixel will have a higher probability of becoming defective, resulting in defect clusters. The distances between defects in a cluster are much shorter than for defects located randomly across the sensor. To demonstrate the lack of clustering in our data, from all the tested cameras, we calculated the distances between defective pixels using the x-y coordinates. Two histogram plots of distances between defects in CCD and APS imagers are shown in Figure 2.

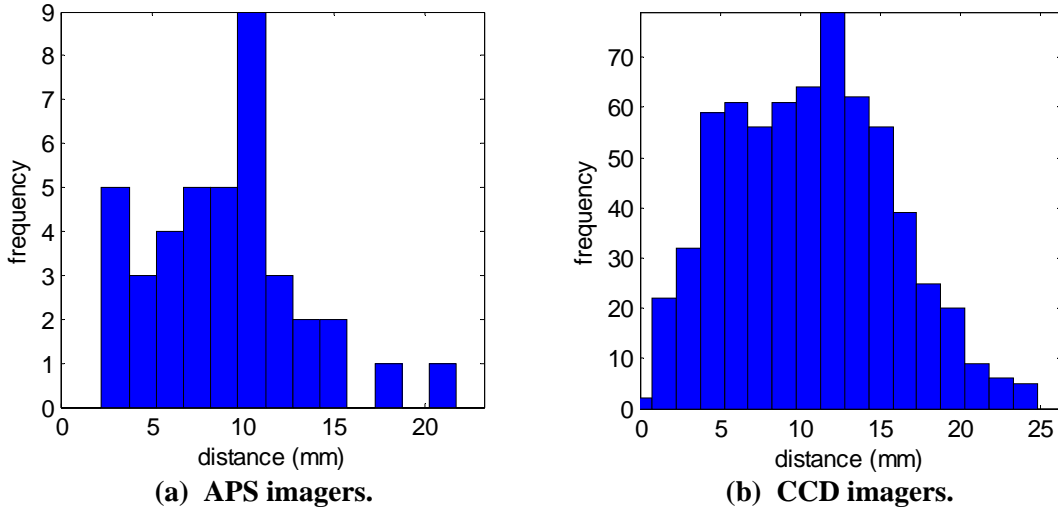


Figure 2. Defect distance distributions from all tested (a) APS, and (b) CCD imagers.

Both plots exhibit similar characteristics in which there is no significant bias toward short or long distances. Both plots have broad distribution and peaks located around 8-10mm on these sensors which are approximately 24 x 16mm. If there existed two or more local areas (clusters) of material problems, the histogram would show a peak at short distances, and another peak of long distances, which do not exist here. In addition, a similar distribution is found for both CCD and APS imagers, suggesting that defects are likely not caused by material failure, but by some external sources of defect mechanism such as radiation.

To further prove that the defects are distributed uniformly over the sensor area, we simulated an array with 9 defects (such as in Figure 1(a)) which were randomly distributed, and calculated the expected frequencies of distances between the defects. We then compared these expected frequencies to the distribution in Figure 2(a). The results are shown in the next table:

Distance (mm)	0 - 4.5	4.5 - 9	9 - 13.5	13.5 - 18	18 - 22.5
Expected frequency	4.7	10.5	11.8	8.9	4.1
Observed frequency	5	12	17	5	1

A Chi-Square test results in a value of 6.58, which is smaller than the critical value of 9.49 (for 4 degrees of freedom). This proves that the defects are actually distributed uniformly over the sensor. We next show, by estimating the defect size, that the defects are isolated and not clustered.

5. Estimating defect size

In Table 3, we show the minimum, average defect distance and pixel dimension collected from all tested cameras.

Table 3. Summary of defects found in tested cameras.

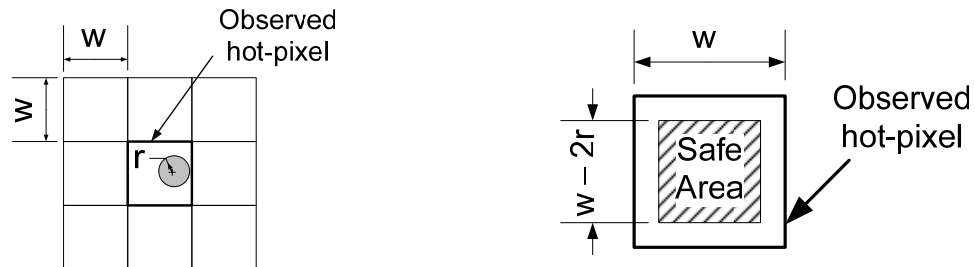
	Minimum distance	Average distance	Average pixel size
APS	2.39 mm	8.97 mm	7.03 x 7.03 μm
CCD	0.65 mm	10.55 mm	6.29 x 8.21 μm

As shown in the table, the shortest distances between defects are 2.39 mm and 0.65 mm in the APS and CCD sensors, respectively. In both sensors, the shortest distance between defects is much larger than one pixel (about 7-10 μm) and is approximately 79-340 pixels. From this result, we can confirm that there are no neighboring defects and that the size of a defect is smaller than the size of a pixel.

We next attempt to place an analytical upper bound on the defect size. The size of hot pixel defects cannot be measured directly. Still, we can infer an upper bound on this size based on the total absence of hot-pixel clusters, since a large-area defect affecting a pixel is likely to influence the characteristics of some of its adjacent neighbors. At each observed hot-pixel location, all 8 neighboring pixels have been characterized in both bright- and darkfield conditions to determine if they too are defective, and no hot-pixel-neighbors were observed to be defective in any of the tested cameras.

To quantitatively estimate the upper bound of the hot pixel defect size, we use the simple model illustrated in Figure 3(a). We treat the image sensor as an array of square pixels of size $w \times w$ each, and assume that the defects are circular spot defects with radius R (which is a random variable). In this first-order approximation, the entire pixel area is sensitive to defects so that a hot-pixel fault is created when any portion of the defect overlaps any portion of the pixel area. The similarity between CCD and APS sensors in developing in-field hot pixels suggests that the causing mechanism may be layout-independent, justifying this basic assumption.

We refer to a hot-pixel with no faulty neighbors as an *isolated fault*. An isolated fault develops only if the center of the defect of radius $R=r$ lands within the hatched *Safe Area* shown in Figure 3(b).



(a) Sensor array with circular spot defects. (b) Pixel area leading to isolated faults.
Figure 3. Hot defect model showing (a) a sensor array with circular spot defects and (b) safe region of a pixel leading to an *isolated fault*.

We now make the assumptions that defects are uniformly likely to land anywhere in the pixel, and that all N observed hot-pixel faults are caused by defects with the same radius $R=r$. The latter assumption is justified by the result, which shows that the defects are indeed very small so that variations in size between defects should also be small. The probability of observing only isolated faults in all N hot-pixel sites is obtained by the following equation,

$$\Pr(N_Isolated_Faults | R = r) = \begin{cases} \left(1 - \frac{2r}{w}\right)^{2N} & r < \frac{w}{2} \\ 0 & r \geq \frac{w}{2} \end{cases} \quad (5)$$

Bayes' theorem can now be used to estimate the probability that the causing defect radius is less than some upper bound r_{max} .

$$\Pr(R \leq r_{max} | N_Isolated_Faults) = \frac{\int_0^{r_{max}} \left(1 - \frac{2r}{w}\right)^{2N} f(r) dr}{\int_0^{w/2} \left(1 - \frac{2r}{w}\right)^{2N} f(r) dr}, \quad (6)$$

where $f(r)$ is some assumed prior probability density function of defect sizes. We first consider the simplest case where defects of all sizes within the range $[0, R_{Upper}]$ are equally likely so that $f(r)$ is the density function

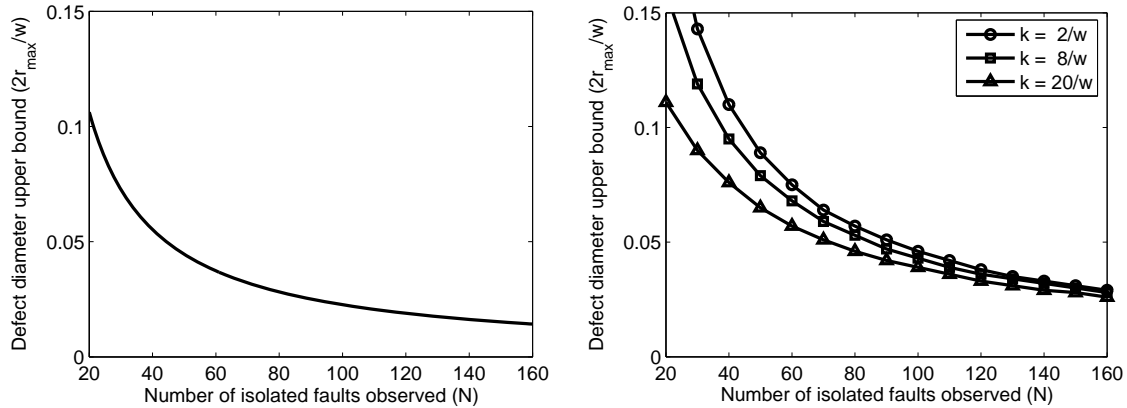
$$f(r)_{Uniform} = \begin{cases} \frac{1}{R_{Upper}} & 0 \leq r \leq R_{Upper} \\ 0 & otherwise \end{cases} \quad (7)$$

Now consider a more complex defect radial distribution, a decreasing prior distribution like the exponential function given in Equation (8) which more realistically parallels the models used in manufacturing yield analysis. Again, we assume that the defect diameter can range from 0 to greater than $2w$ and allow the parameter k of the exponential distribution to be varied.

$$f(r)_{Exponential} = \begin{cases} k \cdot e^{-k \cdot r} & r \geq 0 \\ 0 & otherwise \end{cases} \quad (8)$$

To establish an upper bound on the defect diameter with some confidence level, CL , we choose a particular $f(r)$ and solve (6) for r_{max} by setting $\Pr(R \leq r_{max} | N_Isolated_Faults) = CL$. Figure 4 shows calculated values of $2r_{max}/w$ (a relative defect diameter) for both prior distributions at a conservative 99% confidence level. In the case of the exponential prior distribution, several values of k have been tried, representing an increasingly-condensed distribution function. Both sets of results suggest that hot pixel defects are indeed much smaller than the pixel size. At our current 98 observed isolated faults, the uniform prior distribution case indicates that defect diameter is less than 2.3% of the pixel width (or about 0.2 μm), while the exponential distribution with $k=8/w$ shows that the defect diameter is less than 4.3% of the pixel width (about 0.4 μm).

The fact that either distribution generates an upper bound of very small radius suggested that the defect is nearly point like. This means that the exact distribution model is not very important. In addition, the fact that these are point type defects and the defect rates are about equal in CCD and APS where layouts are different, suggests that these defects are not sensitive to layout characteristics.

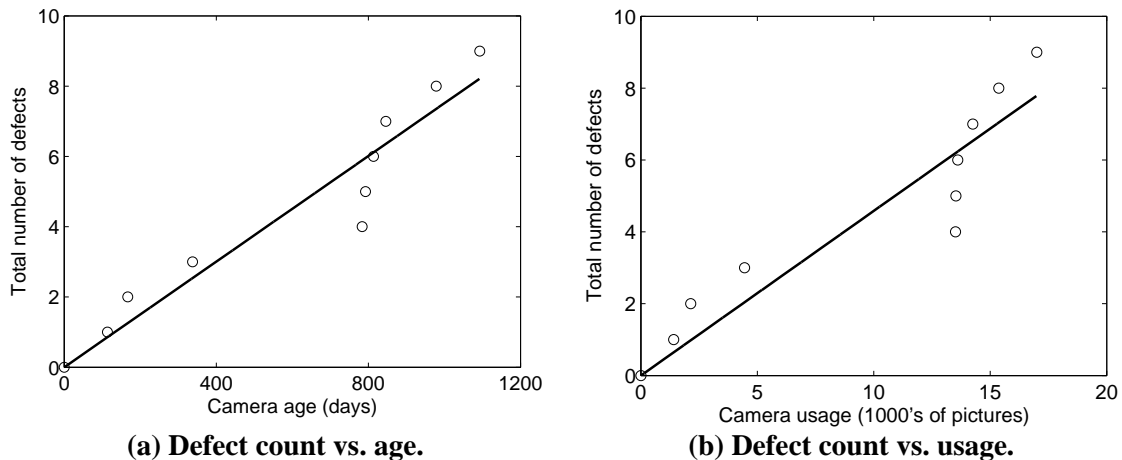


(a) r_{max} with uniform size distribution (b) r_{max} with exponential size distribution
Figure 4. Upper bound on the relative defect diameter for two different prior distributions of defect size: (a) uniform distribution ($R_{Upper} > \frac{1}{2}w$) and (b) decreasing exponential distribution.

6. Temporal growth of defects over sensor lifetime

Defect growth over time can be tracked by examining images taken throughout the lifetime of each camera. Once the location of a defect has been identified by calibration, previously-captured photographs are analyzed for the presence or absence of the defect. The date on which the defect first appears in photos is thus taken as the defect development date. This process is repeated for all known defects and is used to determine growth rate.

Due to the extensive catalog of photographs required by this procedure, defect growth data has been extracted for a single camera only. The development date was identified for each defect discovered in calibrated darkfield testing and results were compiled to indicate the defect density as a function of imager age [2]. The plot of defect growth is presented in Figure 5(a) with respect to the camera age, and in Figure 5(b) with respect to the camera usage (total number of pictures taken). Both plots show a good linear regression fit to the data, from which a defect growth rate of 0.22 defects/month, or 0.52 defects/1000 pictures can be obtained. The accuracy of each defect development date is limited by the availability of suitable photographs; most data points are accurate to within ± 30 days and the worst-case error is limited to ± 56 days.



(a) Defect count vs. age. (b) Defect count vs. usage.
Figure 5. Hot pixel defect growth as a function of (a) camera age, and (b) camera usage for Camera A [2].

These results show a continual growth of defects that do not appear to heal over time. The steady growth rate indicates that defects develop due to a constant stress rather than a single traumatic event such as dropping or heating the camera, and that the sensitivity to defects does not increase with time (in the time frame we considered).

To prove this last point we analyzed the inter-defect times - the times between consecutive defects - for camera A (an APS imager). These times were 9, 21, 32, 53, 114, 114, 133, 171 and 446 days.

The average inter-defect time for camera A is 122 days. By dividing the sample into 3 time intervals, we count the actual number of observations that are less than 49 days, between 49 to 135 days and above 135 days. The actual frequencies are used to compare to the expected frequencies found in an exponential distribution with parameter $k = 1/122$. The results of the above comparison are summarized in Table 4.

Table 4. Comparison of observed and expected distribution.

Inter-defect time (days)	0 - 48	49 - 135	136 -
Observed frequency	3	4	2
Expected frequency	3	3	3

From a Chi-Square test on the observed and expected count, the Chi-Square statistic is found to be 0.66. This small Chi-Square value (compared to the critical value of 5.99 for 2 degrees of freedom) implies that the inter-defect time follows an exponential distribution. Moreover, an exponential distribution of the inter-defect time indicates that the in-field defects occur at a constant rate. In a defect mechanism that is related to material degradation, a cluster of defects will develop at approximately the same time; thus defects will develop at an increasing rate as opposed to a constant rate. With defects occurring at a constant rate, they are again most likely to occur due to a random source such as cosmic ray radiation [1].

7. An alternative approach to defect growth investigation

We next studied the defect growth rate with several more cameras. Previously, the measure of defect growth relied on the availability of a complete set of photographs from each tested camera. The procedure of tracking the occurrence of each defect is cumbersome, and very often we do not have access to the collection of pictures required for this analysis. An alternative approach is to use darkframe taken from each camera. Calibration on the darkframe will give an approximate number of defects at the time the darkframe was taken. By collecting the darkframe from each camera at constant intervals, we can generate a plot of the number of defects with respect to the age of the camera. Figure 6 shows the plot of the defect growth collected from all tested cameras.

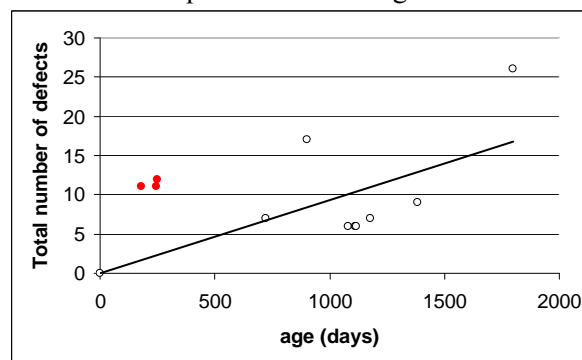


Figure 6. Defect growth of all cameras from a collection of darkframes.

In this plot, a linear function was fit to the above curve excluding the outliers (highlighted dots). The slope of the linear function represents the number of defects developed per day, which is approximate 0.0094/day or 0.28/month. Three of the tested cameras show very high defect rates developed at an early time, and are highlighted in the above plot. What is notable about these is that all three cameras have been taken aboard on many transpacific air flights. It is known that radiation level is 100 times higher in transatlantic/pacific flights, and that has been hypothesized to create higher defect levels. Since no material degradation would show these characteristics, this result is consistent with the discussion on the influence of radiation on image sensors [1].

8. Conclusions

This paper builds on our preliminary investigations, which suggested that imager hot pixel defects are developed individually rather than in clusters. An extensive analysis was performed to gain a better understanding of the distribution and growth of defects. In particular, the distance of separation between defective pixels and the inter-defect time have been measured.

The defect distance results have suggested that defects are distributed uniformly across the sensor area. In fact, the minimum distance of separation between defects was found to be approximately between 79 to 340 pixels. This result has shown that the size of defects is much smaller than the size of a pixel. Furthermore, a similar distribution found in both APS and CCD imagers has indicated that defects are not likely to be caused by material degradation. From a more detailed analytical perspective, with approximately 100 observed isolated defects, the diameter of the defect was shown to be less than 2.3% of a pixel size, or about 0.2 μm , at 99% confidence level.

A detailed analysis on a single camera has shown that the inter-defect time appears to have an exponential distribution with a constant rate. This again suggests that defects are not likely to be caused by material degradation.

Our results have clearly shown that defect development in cameras is so common as to be present in almost every camera that has been in the field for a significant period of time. One important point that the study shows is that analyzing defects in a wide range of cameras is leading toward a better understanding of the cause of these defects. If, as the current evidence suggests, radiation is the source of defects, we should be able to predict defect occurrence rate based on the radiation environment. As an example, the conditions of high radiation in high altitude air travel (transpacific/atlantic flights) may possibly accelerate the defect rate. If proven, this will significantly enhance our prediction on the development of in-field defects for cameras over time. Furthermore, this will help us estimate the reasonable lifetime of the camera before a defect mediation mechanism becomes required on high quality cameras. We are currently conducting a bigger study with a larger number of test cameras over longer periods of time, to further investigate the possible defect mechanisms.

9. References

- [1] A. J.P. Theuwissen, "Influence of Terrestrial Cosmic Rays on the Reliability of CCD Image Sensors," IEDM 2005, San Francisco, CA, 2005.
- [2] J. Dudas, L. M. Wu, C. Jung, G. H. Chapman, Z. Koren and I. Koren, "Identification of in-field defect development in digital image sensors," Proc. SPIE 6502, San Jose, CA, January 2007.